Inorg. Chem. **2007**, *46*, 4960–4967

Naphthylimido-Substituted Hexamolybdate: Preparation, Crystal Structures, Solvent Effects, and Optical Properties of Three Polymorphs

Jian Hao,[†,‡] Laurent Ruhlmann,*[,‡] Yulin Zhu,[†] Qiang Li,[†] and Yongge Wei*[,†]

Department of Chemistry, Tsinghua University, Beijing 100084, P. R. China, and Laboratoire de Chimie Physique, UMR au CNRS 8000, Université de Paris-Sud XI, 1405 Orsay Cedex, France

Received January 14, 2007

$[(n\text{-}C_4H_9)_4N]_2[Mo_6O_{18}(N\text{-}1\text{-}C_{10}H_6\text{-}2\text{-}CH_3)]$ (**1**) has been prepared by the reaction of 1-amino-2-methylnaphthalene hydrochloride with $[(n\text{-}C_4H_9)_4N]_4[\alpha\text{-}Mo_8O_{26}]$ in the presence of 1,3-dicyclohexylcarbodiimide. Three solvent-free crystalline phases are isolated from the mixed solvents of acetone and acetic ether. The X-ray single-crystal structures of the three phases have been determined, showing the packing and supramolecular assembly characters (pseudohigher symmetry, helical chains, and π–π stacking) by which the effect of solvent polarity and crystallization speed on polymorphism in organic–inorganic hybrids has been demonstrated.

Introduction

Polyoxometalates (POMs) formed by the early transition metals constitute a vast class of inorganic cluster systems characterized by an intriguing variety of architectures and topologies and applications in catalysis, biology, magnetism, nanoscience, optics, and medicine.[1] Over the past few years, there has been increasing interest in the chemistry of organically derivatized POMs.[1c,e] Among the organic derivatives of POMs, arylimido derivatives[2,3] with the general formula $[Mo_6O_{19-x}(NAr)_x]^{2-}$ have attracted particular interest because the organic π electrons may extend their conjugation to cluster d electrons, thus resulting in strong d−π interactions. Moreover, the addition of aromatic ligands may introduce some new interactions such as $\pi-\pi$ stacking, Ar−H···O hydrogen bonds,[3] and other intermolecular-bonding interactions[4] by which polymorphism with various crystal packing could occur.

Polymorphism, defined as the ability of some molecules to crystallize into different structural forms,[5,6] is attracting much attention because several packing arrangements or various conformations can result in significant changes of the physical properties of compounds.[7] Most discussions of polymorphism are about small construction units by which one can fully understand intra- and intermolecular interac-

* To whom correspondence should be addressed. E-mail: yonggewei@mail.tsinghua.edu.cn (Y.W.), Laurent.Ruhlmann@lcp.u-psud.fr (L.R.).

† Tsinghua University.

‡ Université de Paris-Sud XI.

(1) (a) Pope, M. T. In *Comprehensive Coordination Chemistry II*; Wedd, A. G., Ed.; Elsevier: Oxford, 2004; Vol. 4, p 635. (b) Hill, C. L. In *Comprehensive Coordination Chemistry II*; Wedd, A. G., Ed.; Elsevier: Oxford, 2004; Vol. 4, p 679. (c) Gouzerh, P.; Proust, A. *Chem. Rev.* **1998**, *98* (1), 77−111. (d) Long, D.-L.; Cronin, L. *Chem.—Eur. J.* **2006**, *12*, 3698−3706. (e) Villanneau, R.; Delmont, R.; Proust, A.; Gouzerh, P. *Chem.—Eur. J.* **2000**, *6*, 1184−1192.

(2) (a) Moore, A. R.; Kwen, H.; Hamaker, C. G.; Mohs, T. R.; Beatty, A. M.; Harmon, B.; Needham, K.; Maatta, E. A. *New Classes of Functionalized Polyoxometalates: Organo-Nitrogen Derivatives of Lindqvist Systems*. In *Polyoxometalate Chemistry for Nano-Composite Design*; Yamase, T., Pope, M. T., Eds.; Kluwer Academic: New York, 2002; pp 129−138. (b) Bar-Nahum, I.; Narasimhulu, K. V.; Weiner, L.; Neumann, R. *Inorg. Chem.* **2005**, *44*, 4900−4902.

(3) (a) Qiu, Y.; Xu, L.; Gao, G.; Wang, W.; Li, F. *Inorg. Chim. Acta* **2006**, *359*, 451−458. (b) Shi, Y.; Lu, X.; Fu, F.; Xue, G.; Hu, H.; Wang, J. *J. Chem. Crystallogr.* **2005**, *35*, 1005−1010. (c) Li, Q.; Wu, P.; Wei, Y.; Wang, Y.; Wang, P.; Guo, H. *Inorg. Chem. Commun.* **2004**, *7*, 524−527. (d) Xu, B.; Peng, Z.; Wei, Y.; Powell, D. R. *Chem. Commun.* **2003**, 2562−2563.

(4) (a) Dunitz, J. D.; Gavezzotti, A. *Angew. Chem., Int. Ed.* **2005**, *44*, 1766−1787. (b) Carter, P. W.; Hillier, A. C.; Michael, D. *J. Am. Chem. Soc.* **1994**, *116*, 944−953. (c) Bone, R. G. A.; Bader, R. F. W. *J. Phys. Chem.* **1996**, *100*, 10892−10911.

(5) (a) McCrone, W. C. In *Polymorphism in Physics and Chemistry of the Organic Solid State*; Fox, D., Labes, M. M., Weissberger, A.; Wiley Interscience: New York, 1965; Vol. II, pp 725−767. (b) Bernstein, J. *Conformational Polymorphism in Organic Solid State Chemistry*; Desiraju, G. R., Ed.; Elsevier: Amsterdam, 1987. (c) Braga, D.; Grepioni, F. *Chem. Soc. Rev.* **2000**, *29*, 229−238. (d) *Cambridge Structural Database*, qualifier "Polymorph". (e) Roy, S.; Banerjee, R.; Nangia, A.; Kruger, G. J. *Chem.—Eur. J.* **2006**, *12*, 3777−3788.

(6) (a) Bernstein, J. *Polymorphism in Molecular Crystals*; Oxford University Press: New York, 2002. (b) Bernstein, J. *Nat. Mater.* **2005**, *4*, 427−428. (c) Herbstein, F. H. *Cryst. Growth Des.* **2004**, *4*, 1419. (d) Blagden, N.; Davey, R. J. *Cryst. Growth Des.* **2003**, *3*, 873. (e) Gavezzotti, A. *CrystEngComm* **2002**, *4* (61), 343. (f) Moulton, B.; Zaworotko, M. J. *Chem. Rev.* **2001**, *101*, 1629−1658. (g) Desiraju, G. R. *Science* **1997**, *278*, 404−405.

(7) (a) Bernstein, J.; Davey, R. J.; Henck, J.-O. *Angew. Chem., Int. Ed.* **1999**, *38*, 3440−3461. (b) Desiraju, G. R.; Paul, I. C.; Curtin, D. Y. *J. Am. Chem. Soc.* **1977**, *99*, 1594−1601. (c) Greer, M. L.; McGee, B. J.; Rogers, R. D.; Blackstock, S. C. *Angew. Chem., Int. Ed.* **1997**, *36*, 1862−1864.

10.1021/ic070064b CCC: $37.00
Published on Web 05/10/2007

tions and the subtle interplay of kinetic and thermodynamic factors and hence explain and design the occurrence of polymorphic modifications.[6] To this date, however, there has not been any detailed discussion on the polymorphism of POMs in the reported literature.[5d,8]

$[Mo_6O_{19-x}(NAr)_x]^{2-}$ can be synthesized by the replacement of terminal oxygen atoms of hexamolybdate $[Mo_6O_{19}]^{2-}$, which has the so-called Lindquist structure by various organic species. After the first discovery of the phosphinimine reaction by Maatta et al.[9] and the organoisocyanates protocol by Errington et al.,[10] Errington and co-workers have further reported the aromatic amines route.[11a] Recently, it has been shown that *N*,*N*′-dicyclohexylcarbodiimide (DCC) dramatically facilitates the aromatic amines reaction.[11b] Moreover, to perfect the DCC method, the α-octamolybdate and protonated aromatic amine have been found more effective than the original reactants.[11c,d]

The aim of this article is to report three polymorphs of a new POM derivative with structural details and attempt to explain their formation from experimental conditions. Because the *o*-alkyl unit on the aryl ring of the arylimido ligand, with electron-donating and steric hindrance effects, can strengthen and effectively protect the Mo−N bonds, 1-amino-2-methylnaphthalene has been selected to prepare a new stable compound, the tetrabutylammonium (TBA^+) salt of 2-methylnaphthylimidohexamolybdate, $[(n\text{-}C_4H_9)_4N]_2[Mo_6O_{18}(N\text{-}1\text{-}C_{10}H_6\text{-}2\text{-}CH_3)]$ (**1**), which contains a conjugation between the d electron system of the POM and the p−π electron system of the double aromatic rings. Herein, three polymorphs of **1** (**1**-α, **1**-β, and **1**-γ) were successfully isolated, and the crystallization conditions of different polymorphs were explored. The **1**-α, **1**-β, and **1**-γ polymorphs present some intriguing structural character such as pseudohigher symmetry simulated in the tertiary structure (**1**-α), three-center hydrogen bonds,[12] and an isolated organic−inorganic hybrid helix chain (**1**-β and **1**-γ) as well as $\pi-\pi$ stacking (**1**-γ). Such structural characteristics of the three polymorphs were explained with various factors, including the formation of structured clusters in solution, interaction between the solute and solvent, and the structure of growing surfaces.

Experimental Section

All the bench manipulations for the syntheses were performed under dry nitrogen gas. Acetonitrile was dried by refluxing in the presence of CaH_2 and was distilled prior to use. 1-Amino-2-methylnaphthalene was obtained from TCI-EP and was used as received. ESI-MS spectra were obtained by using a Finnigan LCQ Deca XP Plus ion trap mass spectrometer (San Jose, CA). Elemental analyses were preformed on a Vario EL analyses system. IR spectra were recorded at 298 K using a Perkin-Elmer FT-IR spectrometer. UV−vis spectra and UV−vis reflectance absorption spectra were measured at 298 K with a Shimadzu 2100S spectrophotometer, using pressed barium sulfate plates to set the 100% reflectance level as a reference of reflectance spectra. ^{1}H NMR spectra were taken on a JNM-ECA300 NMR spectrometer at 298 K.

A mixture of $(TBA)_4[\alpha\text{-}Mo_8O_{26}]$ (0.75 mmol), hydrochloride salt of 1-amino-2-methylnaphthalene (1.0 mmol), and DCC (1.5 mmol) was dissolved in anhydrous acetonitrile (10 mL). The mixture was refluxed under nitrogen for about 8 h, during which the solution turned red and some white solid (*N*,*N*′-dicyclohexylurea) precipitated from the dark-red solution gradually. After filtration at room temperature, the filtrate was evaporated into a dark-red solid, which was recrystallized twice in acetone successively and washed with ethanol. The products were red plate crystals in moderate yield of ca. 60−70%.

ESI-MS, most intense peaks, *m*/*z* (%): 509.2 (100) ([POM − N − Ar]$^{2-}$, calcd, 509.4 u), 1020.3 (15) ([H(POM − N − Ar)]$^-$, calcd, 1019.8 u). Anal. Calcd for $C_{43}H_{81}Mo_6N_3O_{18}$ (1503.75): C, 34.34; H, 5.43; N, 2.79. Found: C, 33.98; H, 5.36; N, 2.59. ^{1}H NMR (300 MHz, DMSO-d_6): δ 0.92 (t, 24H, TBA-δH), 1.33 (sextet, 16H, TBA-γH), 1.55 (quintet, 16H, TBA-βH), 2.83 (s, 3H, CH_3−Ar), 3.15 (t, 16H, TBA-αH), 7.46 (d, 1H, ArH), 7.55 (t, 1H, ArH), 7.66 (m, 2H, ArH), 7.92 (d, 1H, ArH), 8.62 (d, 1H, ArH) ppm. UV−vis (MeCN): λ_{max} = 228, 255, 387 nm. IR (KBr): ν 779(s), 947(s), 974(m), 1377(m), 1466(m), 2870(m), 2959(m) cm^{-1}.

The red plate crystals that crystallized from acetone are the only polymorph β (**1**-β). They were redissolved in a mixed solvent of acetone and acetic ether (1:1) into a saturated solution. The crystallizing speed was controlled by pinholes to volatilize the solvent. Under normal volatilizing speed, three kinds of crystals can form: red plate **1**-β crystals, brown block crystals (**1**-γ), and a few red block crystals (**1**-α). By fast volatilization (in 1 day), **1**-β deposited first, and several hours later a few **1**-α crystals crystallized together with **1**-β. By slow volatilization (over 1 month), block **1**-γ and thick plate **1**-β crystals crystallized together, and sometimes only **1**-γ crystallized! The yield of **1**-α can be increased to ca. 10% via fast volatilization in a dichloromethane−acetic ether (1:2) solution, where three polymorphs deposited together.

Three suitable single crystals were mounted on a glass fiber. The measurements were made on a Rigaku RAXIS-RAPID diffractometer. The data collection was performed at 288(2) K with graphite-monochromated Mo Kα radiation (λ = 0.71073 Å)

(8) (a) Gamelas, J. A. F.; Soares, M. R.; Ferreira, A. A.; Cavaleiro, M. V. *Inorg. Chim. Acta* **2003**, *342*, 16. (b) Roman, P.; Luque, A.; Aranzabe, A.; Gutierrez-Zorrilla, J. M. *Polyhedron* **1992**, *11* (16), 2027−2038.

(9) (a) Du, Y.; Rheingold, A. L.; Maatta, E. A. *J. Am. Chem. Soc.* **1992**, *114*, 345−346. (b) Proust, A.; Thouvenot, R.; Chaussade, M.; Robert, F.; Gouzerh, P. *Inorg. Chim. Acta* **1994**, *224*, 81. (c) Moore, A. R.; Kwen, H.; Beatty, A. M.; Maatta, E. A. *Chem. Commun.* **2000**, 1793−1794.

(10) (a) Clegg, W.; Errington, R. J.; Fraser, K. A.; Lax, C.; Richards, D. G. In *Polyoxometalates: From Platonic Solids to Anti-Retroviral Activity*; Pope, M. T., Müller, A., Eds.; Kluwer: Dordrecht, The Netherlands, 1994; p 113. (b) Strong, J. B.; Ostrander, R.; Rheingold, A. L.; Maatta, E. A. *J. Am. Chem. Soc.* **1994**, *116*, 3601−3602. (c) Mohs, T. R.; Yap, G. P. A.; Rheingold, A. L.; Maatta, E. A. *Inorg. Chem.* **1995**, *34*, 9−10. (d) Stark, J. L.; Young, V. G., Jr.; Maatta, E. A. *Angew. Chem., Int. Ed.* **1995**, *34*, 2547−2548. (e) Strong, J. B.; Yap, G. P. A.; Ostrander, R.; Liable-Sands, L. M.; Rheingold, A. L.; Thouvenot, R.; Gouzerh, P.; Maatta, E. A. *J. Am. Chem. Soc.* **2000**, *122*, 639.

(11) (a) Clegg, W.; Errington, R. J.; Fraser, K.; Holmes, S. A.; SchSfer, A. *J. Chem. Soc., Chem. Commun.* **1995**, 455−456. (b) Wei, Y. G.; Xu, B. B.; Barnes, C. L.; Peng, Z. H. *J. Am. Chem. Soc.* **2001**, *123*, 4083−4084. (c) Xu, L.; Lu, M.; Xu, B. B.; Wei, Y. G.; Peng, Z. H.; Powell, D. R. *Angew. Chem., Int. Ed.* **2002**, *41*, 4129−4132. (d) Wu, P. F.; Li, Q.; Ge, N.; Wei, Y. G.; Wang, Y.; Wang, P.; Guo, H. Y. *Eur. J. Inorg. Chem.* **2004**, *14*, 2819−2822.

(12) (a) Raymo, F. M.; Bartberger, M. D.; Houk, K. N.; Stoddart, J. F. *J. Am. Chem. Soc.* **2001**, *123*, 9264−9267. (b) Hung, C.-Y.; Cabell, L. A.; Anslyn, E. V. *J. Am. Chem. Soc.* **1994**, *114*, 2118−2192. (c) Pihko, P. M. *Angew. Chem., Int. Ed.* **2004**, *43*, 2062−2064. (d) Parra, R. D. *J. Chem. Phys.* **2005**, *122*, 184325/1−8.

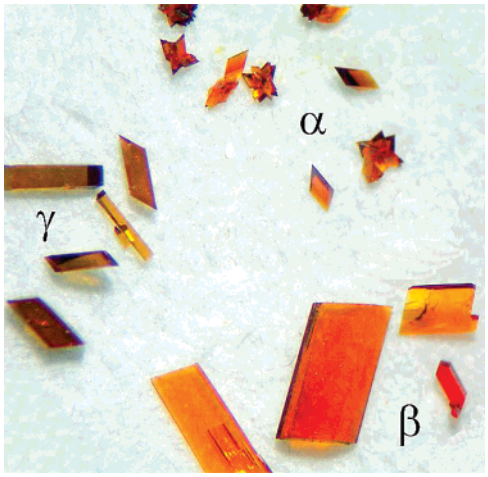

Figure 1. Image highlighting the pattern of three polymorphs.

operating at 50 kV and 80 mA. Absorption corrections were applied based on the symmetry-equivalent reflections. Data reduction was performed by the teXsan for Windows. Both structures were solved by direct methods and refined by the full-matrix least-squares method on F^2 with the SHELXTL software package of version 5.10. CCDC-617137−617139 contain the supplementary crystallographic data for this paper. These data can be obtained free of charge from the Cambridge Crystallographic Data Centre via www.ccdc.cam.ac.uk/data_request/cif.

Results and Discussion

1. Synthesis of Three Polymorphs. The preparation of arylimidohexamolybdate derivatives is now well established. In the DCC method, the efficiency of α-octamolybdate[11c] was improved by the use of a protonated amine[11d] by which the extra proton intensifies the octamolybdate to hexamolybdate conversion. Under different crystallization conditions, compound **1** can crystallize into three crystal polymorphs. The best crystallization condition of **1**-α is a fast crystallization from the 1:2 mixed solutions of dichloromethane and acetic ether. **1**-*β* is easily obtained in pure acetone. However, **1**-*γ* grows slowly from a 1:1 mixed solution of acetone and acetic ether.

2. Molecular Structure and Spectroscopic Studies. Single-crystal structural analysis (Figure 1 and 2 and Table 1) shows that the arylimido ligand is covalently bonded to a terminal position of the hexamolybdate in the three polymorphs of **1**. The short Mo1−N1 distance and collinearity of C1−N1−Mo1 atoms are consistent with a substantial degree of aromatic imido groups bonding and conjugating at an octahedral d^0 metal system.

Similar to many other Lindqvist anions, compound **1** shows the pattern of short/long trans bond alternation in Mo−Ob bond lengths within the equatorial rings as seen in Figure 3.

The ^{1}H NMR spectra of compound **1** showed that the integration matches the molecular structure well. Compared with the corresponding 1-amino-2-methylnaphthalene, all protons of the cluster anion exhibit higher chemical shifts, which are consistent with the electron-withdrawing nature of the Mo−N triple bond. A double peak at about 8.6 ppm shifts much more than other Ar−H (7.5−7.9 ppm) regions

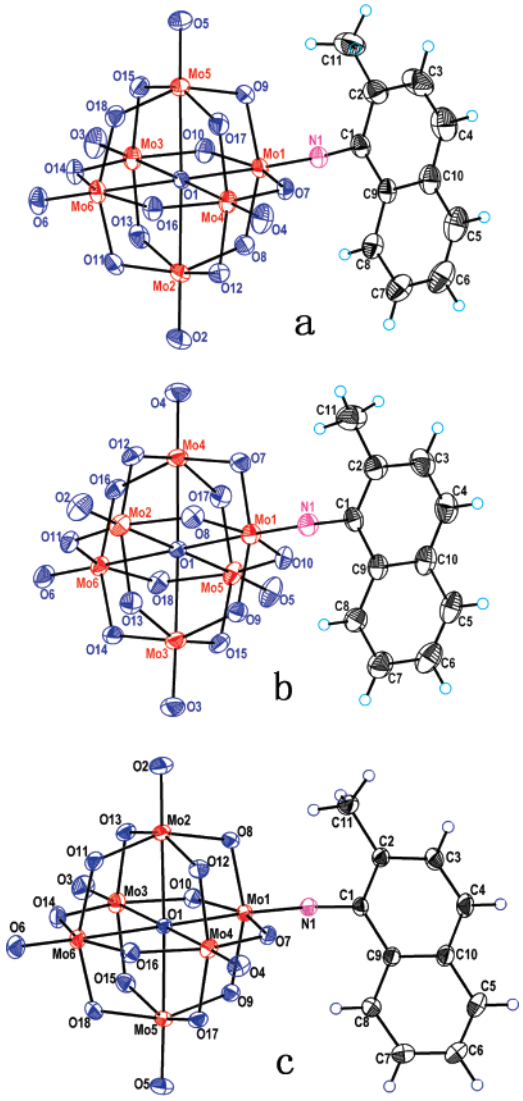

Figure 2. ORTEP drawing of anion structures (a) **1**-α, (b) **1**-*β*, and (c) **1**-*γ*.

Table 1. Selected Bond Lengths (Å) and Angles (deg) for the POM Anions of **1**-α, **1**-*β*, and **1**-*γ*

	1-α	**1**-*β*	**1**-*γ*
Mo1−N1−C1	171.52(1)	177.66(2)	175.46(3)
C1−N1	1.392(1)	1.381(11)	1.378(16)
N1−Mo1	1.740(2)	1.728(14)	1.736(19)
C6−C1−Mo1−Mo2/3/5[a]	−14.58(1)	7.40(1)	26.23(3)

[a] The dihedral angle between the naphthalene plane and the Mo_4 plane; different atom label for **1**-α/**1**-*β*/**1**-*γ*.

and is assigned as the proton in the intramolecular hydrogen bonds that remain in solution whereas the intermolecular hydrogen bonds are destroyed.

The IR spectra of compounds **1** are similar to those of previously reported monoorganoimido derivatives $(TBA)_2[Mo_6O_{18}(N-R)]$.[2,3] The new Mo−N stretching vibration appears at 974 cm^{-1} as a shoulder peak. Compared with the parent hexamolybdate anion, Mo−O stretching and Mo−O_b−Mo asymmetric stretching vibrations bathochromically shift from 957 to 947 cm^{-1} and from 798 to 779 cm^{-1}, respectively, which implies that these bonds weaken to some extent due to the stronger Mo−N bonding interaction than

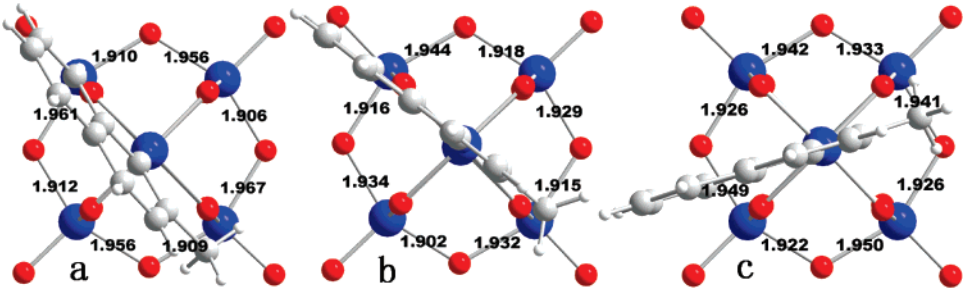

Figure 3. Alternating long/short bonding pattern around the equatorial belt of (a) **1**-α, (b) **1**-*β*, and (c) **1**-*γ*.

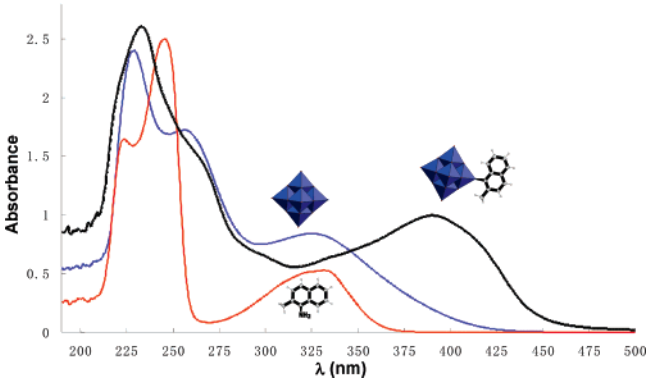

Figure 4. UV−vis absorption spectra (nm) of **1** compared to the hexamolybdate anion and 1-amino-2-methylnaphthalene in CH_3CN.

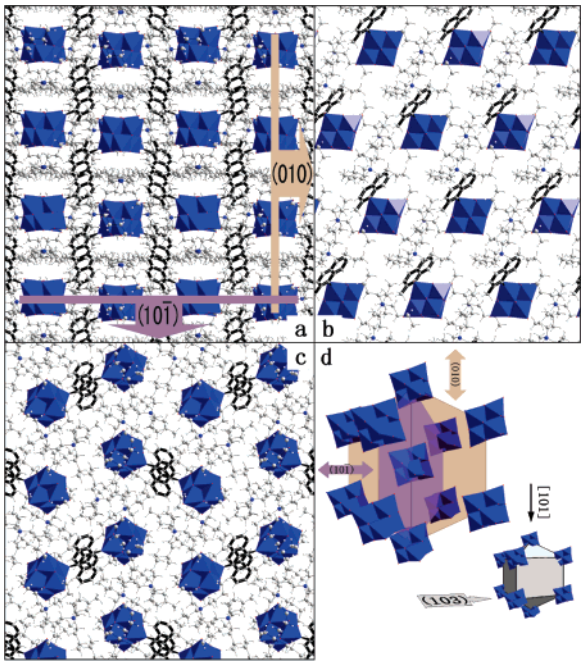

Figure 5. Crystal structure of **1**-α: (a) view along axis [101]; (b) a single plane of (010); (c) a single plane of (10$\bar{1}$); (d) the dodecahedron of the 10 closest POMs to the center POM.

that in Mo−O, whereas the terminal oxo group is replaced by the organoimido ligand. Furthermore, there is not any obvious difference between the IR spectra of the three polymorphs of **1**-α, **1**-*β*, and **1**-*γ*.

The UV−vis absorption spectra of **1**, the parent hexamolybdate anion, and 1-amino-2-methylnaphthalene are shown in Figure 4. Compared with the hexamolybdate anion, a considerable red shift from around 325 to 387 nm accompanied by an increase of the absorption intensity indicates

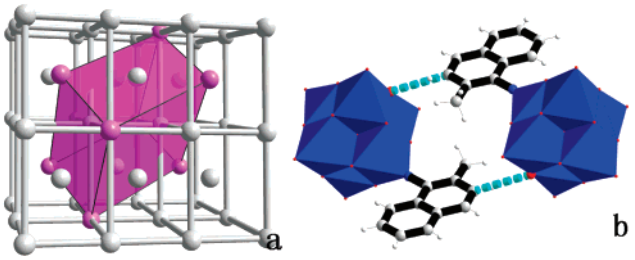

Figure 6. Special structures of **1**-α: (a) real unit cell fits in a pseudo-BCT lattice; (b) dimeric POM anions via hydrogen bonds.

a LMCT band, i.e., the electron transition from the aromatic *π*-type HOMO to the molybdenum d-type LUMO.

3. Comparison of the Three Crystal Structures. Selected crystal data of **1**-α, **1**-*β*, and **1**-*γ* are presented in Table 2.

3.1. Crystal Structure of 1-α. As can be seen in Figure 5, the POM anions of **1**-α prefer an almost equidistant arrangement. Every POM is surrounded by 10 closest POMs, which form a dodecahedron. The distances between the center and vertex POMs are approximately equal: 11.55(2), 11.60(2), 11.77(17), 11.77(17), 12.61(6), 12.61(6), 12.78(16), 12.78(16), 12.96(1), and 12.96(1) Å. Herein, the distances are measured by O1 atoms, i.e., the centers of every POM clusters.

Undoubtedly, in **1**-α, there is not any 3-fold, 4-fold, or 6-fold rotation symmetry axis, which can be illusively found by a glimpse at Figure 5. This illusive symmetry is the pseudohigher symmetry simulated in the tertiary structure. Generally, the approximate symmetry can be realized under ignoring, thinly moving, or changing certain atoms and/or forcibly changing some cell parameters to special values, but without changing the main state of a cell. Oppositely in the case of **1**-α, the higher symmetry only exists in the tertiary structure and would disappear in any structural details. The [101] axis and (103) plane do not have a direct relation normally, but here the angle between them is very close to 90° (89.02°), and in a pseudo-BCT lattice they become the [001] axis and (001) plane (Figure 5d). The indirect relationship between the real lattice and the pseudolattice is shown in Figure 6a. Distinctly observable, none of the edges or surfaces are parallel between the real cell and the pseudocell.

Being different from **1**-*β* or **1**-*γ*, there are always several (ca. 5−10) single crystals of **1**-α growing together (Figure 1), so very few isolated single crystals can be found. This is in accordance with the similar aspect of **1**-α in different directions. Around the quasi-symmetrically arranged

Table 2. Crystal Data of **1**-α, **1**-*β*, and **1**-*γ*

	1-α	**1**-*β*	**1**-*γ*
formula	$C_{43}H_{81}Mo_6N_3O_{18}$	$C_{43}H_{81}Mo_6N_3O_{18}$	$C_{43}H_{81}Mo_6N_3O_{18}$
fw	1503.75	1503.75	1503.75
cryst syst	monoclinic	monoclinic	triclinic
space group	$P2_1/n$	$P2_1/c$	$P\bar{1}$
a (Å)	12.957(3)	13.005(3)	11.480(2)
b (Å)	20.993(4)	22.680(5)	12.391(3)
c (Å)	20.870(4)	19.890(4)	21.288(4)
α (deg)	90	90	76.60(3)
β (deg)	95.27(3)	104.57(3)	77.37(3)
γ (deg)	90	90	89.91(3)
cell volume (Å^3)/*Z*	5653(2)/4	5678(2)/4	2870.6(10)/2
density (g/cm^3)	1.767	1.759	1.740
μ(mm^{-3})	1.358	1.352	1.337
F(000)	3024	3024	1512
cryst size (mm^3)	0.3 × 0.1 × 0.1	0.5 × 0.4 × 0.1	0.5 × 0.2 × 0.1
θ(min, max) (deg)	3.07, 26.00	3.10, 26.00	3.01, 26.00
h, *k*, *l* (min, max)	(−15, 15), (−25, 25), (−23, 25)	(−15, 16), (−27, 27), (−24, 24)	(−14, 14), (−15, 15), (−25, 26)
reflns collected	46 416	46 812	24 908
independent reflns	11 077	11 109	11 228
R_{int}	0.0290	0.1009	0.0216
completeness to $\theta = 26°$ (%)	99.8	99.6	99.5
trans (max, min)	0.8762, 0.6862	0.8767, 0.5513	0.8779, 0.5545
data/restraints/params	11077/0/650	11109/0/631	11228/0/631
GOF on F^2	1.037	0.852	1.053
final *R* indices [$I > 2\sigma(I)$]	$R_1 = 0.0309$	$R_1 = 0.0403$	$R_1 = 0.0317$
	$R_2 = 0.0720$	$R_2 = 0.0698$	$R_2 = 0.0751$
R indices (all data)	$R_1 = 0.0463$	$R_1 = 0.0641$	$R_1 = 0.0370$
	$R_2 = 0.0781$	$R_2 = 0.0774$	$R_2 = 0.0770$
$\Delta\rho$(max, min) (e·Å^{-3})	0.537, −0.531	0.993, −1.799	0.392, −0.842

Table 3. C−H···O Hydrogen Bonds between Anions in Three Polymorphs[a]

		H···O (Å)	C···O (Å)	C−H···O (deg)
1-α	O15···C3	2.662(2)	3.374(2)	146.86(2)
	O4···C6	2.88(1)	3.784(18)	133.89(2)
1-*β*	O2···C6	2.583(14)	3.302(11)	134.49(2)
	O2···C5	2.931(6)	3.463(2)	117.78(2)
1-*γ*	O3···C7	2.705(31)	3.381(54)	130.21(3)
	O3···C6	2.942(48)	3.494(64)	119.40(3)
	O13···C11	2.715(19)	3.668(30)	171.50(2)
	O13···C3	3.044(63)	3.877(79)	150.06(3)

[a] Examples of long C−H···O hydrogen bonds can be found in ref 3.

inorganic clusters, organic ligands, and TBA cations, the equidistant interstices fill to form an oleophilic coating for POM anions. The dimeric structure is regular in arylimido derivatives of POMs.[2,3] In the plane (10$\bar{1}$) of **1**-α (Figure 5c), a dimeric structure conjoined by a couple of Ar−H···O hydrogen bonds (C3−H···O15, 3.374 Å) between cluster anions was also found (Figure 6b). In addition, a set of weaker C−H···O hydrogen bonds, revealed by the important distance of C6−H···O4 (3.784 Å), link the cluster anions to form a 1D chain along the *b* axis. Such long C−H···O hydrogen bonds have also been observed in the literature before.[3]

3.2. Crystal Structure of 1-*β*. In polymorph **1**-*β*, two hydrogen bonds between the cluster anions are deduced from analysis of the X-ray structures. One is between C6 and O2, which is the strongest hydrogen bond in all three polymorphs, and the other is between C5 and O2 (Table 3). The two hydrogen-bonding carbon atoms, C5 and C6, share the same oxygen atom O2, accompanying the formation of the C5−H···O2···H−C6 cycle (Figure 7a), which follows the previously reported model structure based on a quantum chemistry study.[12a] Because the hydrogen bonds tend to arrange in a straight line, there is some tension in such a cycle, which pushes all atoms to locate on the same plane. Indeed, the coplanarity to some extent was really observed as the dihedral angle between the C5−C6−O2 plane and the aromatic plane, equal to 177.8(3)°, which is strong evidence for the duality of O2 in the formation of these hydrogen bonds: the stronger hydrogen bond bends directly toward the second H. Although the second hydrogen bond is obviously weaker, it does play a role in the location of the cluster anions.

By double hydrogen bonds, the cluster anions are connected head-to-tail and form helical chains along the crystallographic *b* axis in **1**-*β*, as shown in Figure 7. Every turn of helices repeats two anions, in which the inorganic clusters, aromatic ligands, and double hydrogen bonds compose the helix together.

Helical structures, known as one of the most interesting superstructures in the context of spontaneous chiral resolution from achiral components, have been extensively explored in the fields of polymorphism[13] and POM chemistry,[14]

(13) (a) Kobayashi, K.; Sato, A.; Sakamoto, S.; Yamaguchi, K. *J. Am. Chem. Soc.* **2003**, *125*, 3035−3045. (b) White-Morris, R. L.; Olmstead, M. M.; Balch, A. L. *J. Am. Chem. Soc.* **2003**, *125*, 1033−1040. (c) Zhang, J.-P.; Lin, Y.-Y.; Huang, X.-C.; Chen, X.-M. *Chem. Commun.* **2005**, 1258−1260. (d) Chen, X.-D.; Dub, M.; Mak, T. C. W. *Chem. Commun.* **2005**, 4417−4419. (e) Stocker, F. B.; Troester, M. A.; Britton, D. *Inorg. Chem.* **1996**, *35*, 3145−3153.

(14) (a) Shi, Z.; Feng, S.; Gao, S.; Zhang, L.; Yang, G.; Hua, J. *Angew. Chem., Int. Ed.* **2000**, *39* (13), 2325−2327. (b) Soghomonian, V.; Chen, Q.; Haushalter, R. C.; Zubieta, J.; O'Connor, C. J. *Science* **1993**, *259*, 1596−1599. (c) Lu, C.-Z.; Wu, C.-D.; Lu, S.-F.; Liu, J.-C.; Wu, Q.-J.; Zhuang, H.-H.; Huang, J.-S. *Chem. Commun.* **2002**, 152−153.

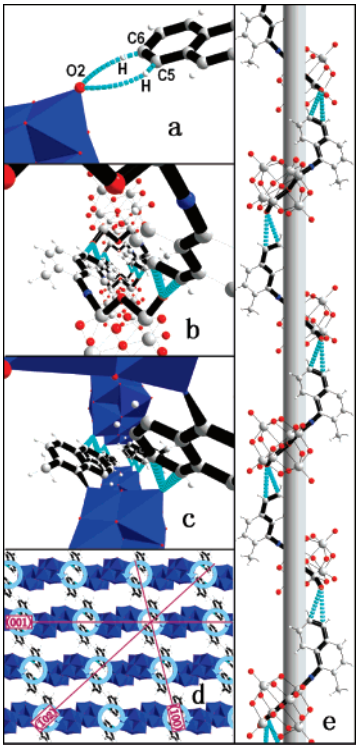

Figure 7. Helical chain in **1**-β: (a) double inter-POM hydrogen bonds; (b, c) view of a singe helix along the crystallographic *b* axis; (d) view of arrangement of helices along the *b* axis; (e) view of a singe helix perpendicular to the *b* axis.

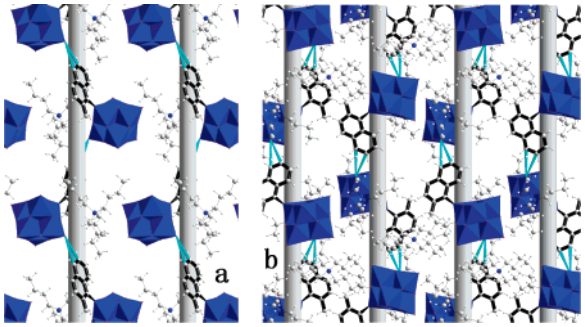

Figure 8. (a) Single plane of (001). (b) Single plane of (100) for **1**-β.

including some organic or inorganic helices in organic−inorganic hybrid compounds. Nevertheless, to our knowledge, no helix composed of a really organic−inorganic hybrid isolated chain was found. Here, in the **1**-β polymorph, the helix is surrounded by cations without any bonding interaction as strong as the intrahelix force, so the helices form the very framework of the **1**-β crystal (Figure 8). The isolatism of the helix is important because in some 3D network structures, e.g., diamonds, the trivial helices can be easily found. On the other hand, the inorganic clusters and organic ligands occupy certain parts of the helical chain in **1**-β. As shown by the thick bonds in parts b−e of Figure 7, the repetitive unit of the main chains is O−Mo−O−Mo−N−C−C−C−C−C−H, with undoubted organic and inorganic parts.

As shown in Figure 7d, both left-handed and right-handed helical chains have been orderly arranged in the same crystal of **1**-β: there are parellel helical chains in the (001) plane (Figure 8a) and an alternating left-right-handed helix in the (100) plane (Figure 8b) or the ($\bar{1}$02) plane. The alternation causes the racemization, which is in agreement with the centrosymmetric space group of the **1**-β crystal.

3.3. Crystal Structure of 1-γ. Being different from the above two polymorphs **1**-α and **1**-β, however, there is another intermolecular interaction, that of $\pi-\pi$ stacking, found to form the POMs dimer in **1**-γ. In such a dimer (Figure 9), two face-to-face naphthyls are well-overlapping with a quite standard $\pi-\pi$ interplanar distance of 3.470 Å. The two aromatic planes are absolutely parallel because they are related each other by an inversion center.

Similar to the case of the **1**-β polymorph, there are also two different three-center hydrgoen bonds observed in **1**-γ (Table 3). The C7−H···O3···H−C6 hydrogen bond (see inset of Figure 9b) is almost the same as that in **1**-β, just a little weaker, and the C3−H···O13···H−C11 bond is even weaker, because an H atom is attached to the sp^3 C11 atom, although the tension is minor in the six-membered cycle. As shown in Figure 9b, all these hydrogen bonds link the $\pi-\pi$ dimers into a 1D chain along the *a* axis. The arrangement under $\pi-\pi$ stacking and multiple hydrogen bonds renders the **1**-γ structure more rigid; thus, **1**-γ has to tolerate more interstices that reduce its crystal density (Table 2).

A comparison between the UV−vis reflectance absorption spectra (Figure 10) of the three polymorphs of **1**-α, **1**-β, and **1**-γ shows the expansion effect of conjugation caused by the $\pi-\pi$ stacking interactions in **1**-γ: compared with the **1**-α and **1**-β polymorphs, two peaks in the visible region both have red-shifted and obviously broadened. Moreover, the HOMO−LUMO peak becomes strengthened. This provides some evidence for the influence of $\pi-\pi$ stacking interactions on the spectra of $\pi-$d conjugated molecules in the solid state.

The reflectance absorption spectra of the powder samples obtained from pure monocrystals of the three polymorphs all present great red shift to about 600 nm compared with the UV−vis absorption spectra of **1** in a CH_3CN solution, where no $\pi-\pi$ stacking interactions and no Ar−H···O hydrogen bonds were observed (Figure 4). The polymorphism properties are present only in the solid state whereas in solution no interaction occurred, as confirmed by ^{1}H NMR spectroscopy (see the Experimental Section). For the $\pi-\pi$ conjugated system, as we know, better coplanar structure leads to greater red shift.[15] However, for the d−π conjugated system here, the coplanar effect is not so important: considering the data in Table 1 and Figure 10, the polymorph

(d) Lu, J.; Xu, Y.; Goh, N. K.; Chia, L. S. *Chem. Commun.* **1998**, 2733−2734. (e) Maggard, P. A.; Stern, C. L.; Poeppelmeier, K. R. *J. Am. Chem. Soc.* **2001**, *123*, 7742−7743. (f) An, H.-Y.; Wang, E.-B.; Xiao, D.-R.; Li, Y.-G.; Su, Z.-M.; Xu, L. *Angew. Chem., Int. Ed.* **2006**, *45*, 904−908.

(15) (a) Biedermann, P. U.; Stezowski, J. J.; Agranat, I. *Chem.−Eur. J.* **2006**, *12*, 3345−3354. (b) Yu, L.; Stephenson, G. A.; Mitchell, C. A.; Bunnell, C. A.; Snorek, S. V.; Bowyer, J. J.; Borchardt, T. B.; Stowell, J. G.; Byrn, S. R. *J. Am. Chem. Soc.* **2000**, *122*, 585−591.

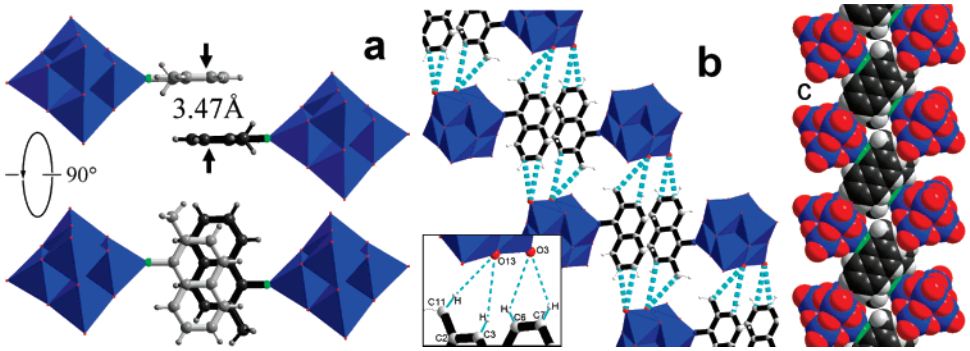

Figure 9. (a) $\pi-\pi$ stacking dimer. (b) Hydrogen bonds between dimers. (c) Dimer chain for **1**-γ.

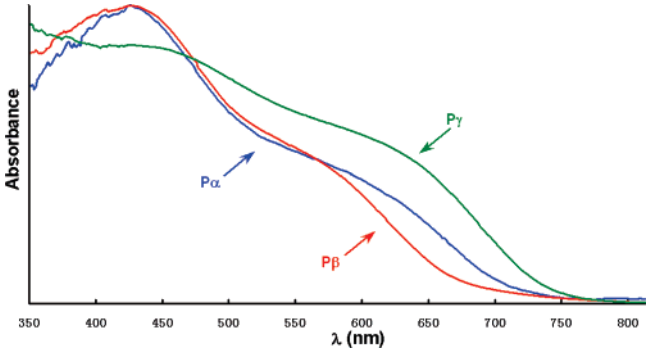

Figure 10. UV−vis absorption spectra (nm) of normalized UV−vis reflectance absorption spectra of the three polymorphs (powder obtained from pure single crystals of **1**-α, **1**-β, and **1**-γ).

Table 4. Coulomb Interactions: the Arrangement of Electric Charges

	TBAs ∼ adjacent POMs (Å)			TBA ∼ plane[a]
1-α: TBA1	6.50(4)	6.78(4)	9.00(1)	0.11
1-α: TBA2	6.75(8)	6.97(0)	7.14(7)	0.34
1-β: TBA1	6.71(4)	6.81(5)	7.09(5)	0.20
1-β: TBA2	6.50(1)	6.84(5)	7.87(3)	0.35
1-γ: TBA1	6.68(10)	6.87(10)	7.23(8)	1.79
1-γ: TBA2	6.35(4)	6.47(5)	9.13(18)	0.92

[a] Distances from TBAs to the plane of three adjacent POMs.

1-γ presents more red shifts than polymorphs **1**-α and **1**-β whereas the coplanarity of **1**-γ presents the least (Figure 3). That might be explained by the presence of important $\pi-\pi$ stacking interactions for **1**-γ.

3.4. Coulomb Interactions. In inorganic ionic crystals, small cations tend to fill smaller interstices if space permits, due to the lower Coulombic potential energy in such interstices. For example, the Coulombic potential energy in a triangle interstice is lower than that in a tetrahedral interstice. In our complicated ionic crystals, this fundamental rule was reconfirmed in an interesting way.

To simplify the distribution of ions and the O1, N2, and N3 atoms, the charge centers of the cluster anion and two TBA cations were chosen to represent the corresponding ions. Under such an approximation, the TBAs of **1**-α and **1**-β were found right in the triangle interstices of three adjacent POMs (Figure 11), because the distances from the TBAs to the plane of the three adjacent POMs are very short.

As shown in Table 4, being different from those of **1**-α or **1**-β, the TBAs in **1**-γ deviate considerably from such triangle interstices. Therefore, on the surface of crystal

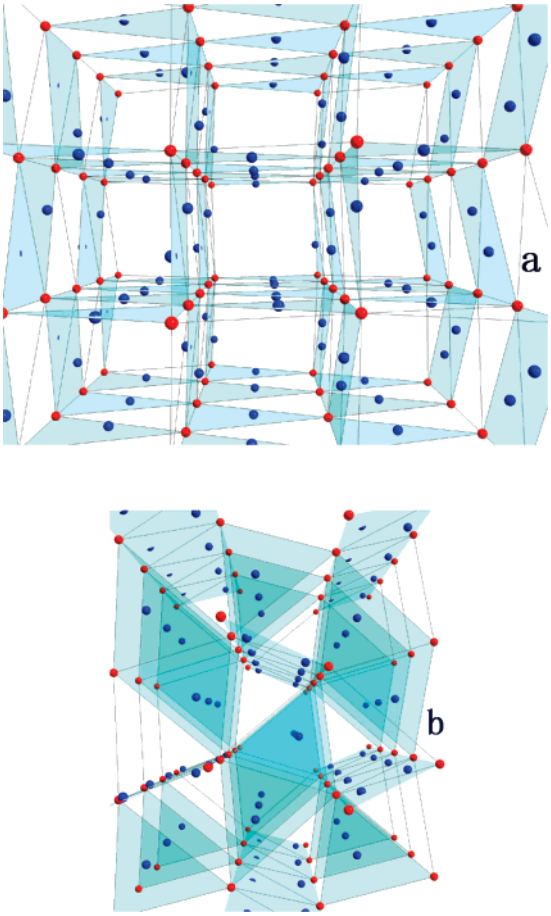

Figure 11. Packing of ions in crystal lattices (red O1 and blue N2 and N3 atoms stand for charge centers of POMs, TBA1, and TBA2, respectively): (a) view along the axis [101] of **1**-α; (b) view along the axis [100] of **1**-β.

growth, they cannot be well fixed by corresponding anion triangles and somehow oscillate around the equilibrium position, so that an energy barrier forms and they take more time to form **1**-γ.

3.5. Relationships between Crystal Structures and Crystallization Conditions. Although three polymorphs can deposit from the same solution at the same temperature and pressure, their crystallization conditions are subtly different. Several experiences indicate the following: (i) **1**-α tends to crystallize in a weaker polar solution under faster crystallization; (ii) **1**-β tends to crystallize in a stronger polar solution; and (iii) **1**-γ tends to crystallize under slower crystallization in a weaker polar solution. Usually, the

different crystal packing arrangements of polymorphs result from different conditions of crystallization. In this report, we can also observe some relationships between crystal structures and crystallization conditions that could be explained by kinetic and energetic factors: (i) The exclusive formation of **1**-α needs very fast crystallization and leads to a pseudohigher symmetry that quasi-equalizes the distribution of the ion charge. (ii) **1**-*β* crystallizes from a stronger polar solution. In this case, **1**-*β* contains a polar chain (head-to-tail) instead of the centrosymmetric dimer in **1**-α and **1**-*γ*; moreover, **1**-*β* possesses the strongest hydrogen bonds in the group of three polymorphs. (iii) Finally, only **1**-*γ* needs very slow crystallization, which suggests that some kinetic barriers of crystallization act as the strong geometrical requirements of $\pi-\pi$ stacking and deviation of the TBA^+ molecule from the anion-triangle interstices.

Conclusion

In summary, we have successfully synthesized a novel arylimido derivative of the hexamolybdate ion, which crystallizes into three polymorphs. Each packing mode in the three polymorphs presents unique character: pseudohigher symmetry, helical chains, and $\pi-\pi$ stacking. These structural motifs suggest that such an organic−inorganic hybrid could arrange into various crystalline solids by virtue of its complicated intermolecular forces, especially those of hydrogen bonds, $\pi-\pi$ stacking, and Coulomb interactions. The effect of crystallization conditions on the polymorphism in organic−inorganic hybrids has been tentatively explained with kinetic and energetic factors. The relationships depicted in this paper may extend to other organic−inorganic hybrids, thus opening a new domain in the crystal engineering of organic derivatives of POMs.

Acknowledgment. This work is supported by NFSC Grants 20671054 and 20373001, by the CNRS, by the Tsinghua Basic Research Foundation No. JCqn2005039, by the University Paris-Sud XI, and by the ANR agency (Grant ANR-05-52437).

Supporting Information Available: Three CIF files. This material is available free of charge via the Internet at http://pubs.acs.org.

IC070064B